minerals

MDPI

Article

Towards Identification of Zircon Populations in Permo-Carboniferous Rhyolites of Central Europe: Insight from Automated SEM-Mineral Liberation Analyses

Arkadiusz Przybyło [1,*], Anna Pietranik [1], Bernhard Schulz [2] and Christoph Breitkreuz [3]

[1] Instytut Nauk Geologicznych, Uniwersytet Wrocławski, pl. Maksa Borna 9, 50-204 Wrocław, Poland; anna.pietranik@uwr.edu.pl
[2] Institut für Mineralogie, Lagerstättenlehre und Petrologie, TU Bergakademie Freiberg, Brennhausgasse 14, 09599 Freiberg/Sachsen, Germany; bernhard.schulz@mineral.tu-freiberg.de
[3] Institut für Geologie, TU Bergakademie Freiberg, Bernhard von Cotta Str. 2, 09599 Freiberg/Sachsen, Germany; cbreit@geo.tu-freiberg.de
* Correspondence: arkadiusz.przybylo@uwr.edu.pl

Received: 24 February 2020; Accepted: 28 March 2020; Published: 30 March 2020

Abstract: Zircon is a main mineral used for dating rhyolitic magmas as well as reconstructing their differentiation. It is common that different populations of zircon grains occur in a single rhyolitic sample. The presence of both autocrystic and antecrystic zircon grains is reflected in their strongly varied chemical compositions and slight spread of ages. However, postmagmatic processes may induce lead loss, which is also recorded as a spread of zircon ages. Therefore, new approaches to identify different zircon populations in rhyolitic rocks are needed. In this study, we suggest that detailed examination of zircon positions in the thin sections of rhyolitic rocks provides valuable information on zircon sources that can be used to identify autocrystic and antecrystic zircon populations. Automated Scanning Electron Microscope (SEM) analyses are of great applicability in determining this, as they return both qualitative and quantitative information and allow for quick comparisons between different rhyolite localities. Five localities of Permo-Carboniferous rhyolites related to post-Variscan extension in Central Europe (Organy, Bieberstein, Halle, Chemnitz, Krucze) were analyzed by automated SEM (MLA-SEM). The samples covered a range of Zr whole rock contents and displayed both crystalline and glassy groundmass. Surprisingly, each locality seemed to have its own special zircon fingerprint. Based on comparisons of whole rocks, modal composition and SEM images Chemnitz ignimbrite was interpreted as containing mostly (or fully) antecrystic zircon, whereas the Bieberstein dyke was shown to possibly contain both types, with the antecrystic zircon being associated with disturbed cumulates. On the other hand, Organy was probably dominated by autocrystic zircon, and Krucze contained dismembered, subhedral zircon in its matrix, whereas Halle zircon was located partly in late veins, filling cracks in laccolith. Both localities may, therefore, contain zircon populations that represent later stages than the crystallization of the main rhyolitic body.

Keywords: volcanic rock structure; subvolcanic; pyroclastic; zircon associations; zircon saturation; mineral liberation analysis (MLA)

1. Introduction

Magmatic accessory minerals may crystallize during different episodes of magma formation and differentiation. This is particularly true for zircon, which can represent crystals formed in contemporary magma (autocryst), crystals formed in earlier magmatic episodes (antecrysts), unresorbed remnants

(inherited or xenocrystic) derived from their source or assimilated rock, or secondary zircons from Zr-enriched fluids that infiltrate rocks [1–4]. The abundance of inherited zircon can be fairly easily identified using Scanning Electron Microscope (SEM) analysis, and confirmed by in situ zircon dating. On the other hand, antecrysts are not that easily identified in SEM images, and can not be distinguished from the main crystallization age by in situ dating techniques, especially in rocks older than 100 Ma, as they are only slightly older than the eruption/solidification. Antecrysts, if identified, provide information on magmatic activity that may not be represented as igneous rocks in the area. Therefore, more-complete pictures of magmatic processes may be obtained if antecrysts are analyzed as what they truly are (i.e., records of a longer period of magma evolution than the rhyolitic rock itself) [5]. The presence of antecrysts can be detected using a strict protocol based on detailed chemical and isotopic analysis [3]. However, we propose that another way to identify different zircon populations is through the careful examination of thin sections of rock to find zircon occurring in different structural positions [6]. To achieve this, automated detection is helpful to obtain a representative catalogue of zircon populations. So far, automated Scanning Electron Microscope Mineral Liberation Analysis (SEM-MLA) has been applied in the industry for solving problems of ore mineral processing and extraction [7]. However, there are other assets of automated SEM methodology, including the detailed modal analysis of different rocks [8,9] or quantification of environmental weathering [10,11]. The great asset of automated SEM analyses is that they do not only calculate modal proportions, but also provide detailed quantitative information on grain size distribution, mineral associations, and phase characteristics such as angularity or length/breadth ratio. Further, the information is retrieved for most of the grains occurring in thin sections of rhyolites. In this paper, we use automated SEM analysis (SEM-MLA) of five different rhyolites (lava dome, dyke, laccolith, lava, and ignimbrite) in order to characterize the zircon microstructural contexts in these rhyolites and to evaluate if they can be interpreted in terms of different zircon populations. Rhyolites often contain mixed autocrystic and antecrystic zircon cargos [1,3–5,12,13] and any technique that facilitates the recognition of these populations provides additional information on the origin of rhyolite magma. This in turn may be important to improving the understanding of zircon ages in rhyolitic rocks [14].

2. Sampling and Methodological Approach

Five rhyolites representing different types of (sub-)volcanic rocks were chosen for petrological and geochemical analyses (Figure 1).

2.1. Bulk Rock Geochemistry

Samples from Organy (n = 6), Bieberstein (n = 6), and Krucze (n = 6) were analyzed in Bureau Veritas Commodities Canada Ltd. by ICP-MS. Chemical composition of bulk rock samples from Chemnitz and Halle were taken from the literature (n = 10, n = 22) [9,15]. The precision for major elements was from 0.11% Relative Standard Devation (RSD) for SiO_2 from Organy to 2.44% RSD for TiO_2 from Krucze. The precision for trace elements was below 5% RSD for the majority of elements (Supplementary Materials Table S1). The accuracy of analysis was below 3% for major elements and below 10% for trace elements.

2.2. Mineral Liberation Analyses

Six polished petrographic thin sections from the least altered samples were analyzed by SEM-MLA, including two sections from Organy and one from each of the other localities. SEM-MLA measurements were performed at the Geometallurgy Laboratory at TU Bergakademie Freiberg with an FEI Quanta 650F SEM-MLA that was equipped with two Bruker Quantax X-Flash 5030 EDX detectors (analysis conditions: E = 25 kV at spot size = 5.0 µm, beam current = 10 nA). Additionally back-scattered electron (BSE) images were collected using this instrument and the JEOL SEM at the University of Wrocław.

Calibration of the BSE greyscale with contrast and brightness was performed using the FEI Quanta 650F SEM-MLA with a copper reference. After automated image analysis, the electron beam was

directed into the centers of contiguous mineral grains characterized by their BSE grey values, and a single Energy-Dispersive X-ray (EDX) spectrum was obtained (XBSE measurement mode). A grid of single EDX spectra was gained from each contiguous domain with distinct BSE grey values (GXMAP measurement mode). Each gained EDX spectrum was normalized by the counting rates $(cts/s)_N$ of the coupled EDX detectors and plotted against the keV scale. These EDX spectra have characteristic peaks at distinct positions in the keV scale and distinct relative cts/s, allowing identification of the major elements present and providing a semiquantitative indication of their concentrations. The SEM-MLA software (version MLA 3.1 by FEI) recognizes each mineral phase after its EDX spectrum by comparison to a reference set of EDX spectra from identified mineral phases with known compositions [7,8]. The mode of recognition is straightforward for phases larger than several microns, but this is not always the case for the rhyolitic matrix. Therefore, in this study, the matrix was defined as three different mixtures of K-feldspar, quartz, albite, and glass (matrix1, matrix2, matrix3). Real matrix in analyzed samples was most often quartz and K-feldspar or glass, which the automated software recognized as either the matrix mixture or the actual mineral. Therefore, to define the proportion between the matrix and phenocrysts, JMicroVision software was used.

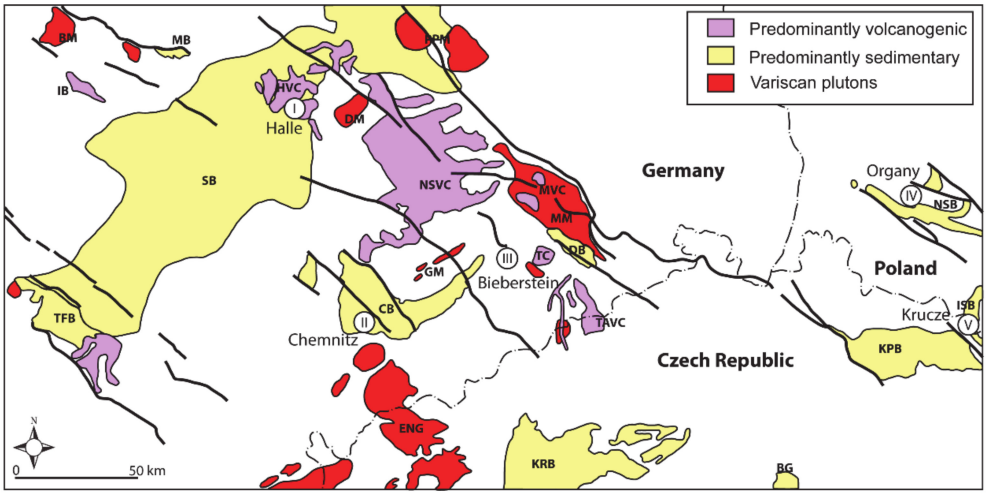

Figure 1. Distribution of Permo-Carboniferous volcanic rocks in Central Europe. Sampling sites: I—Halle Volcanic Complex (Landsberg laccolith), II—Chemnitz Basin–ignimbrite sampled near Zwickau, III—Bieberstein subvolcanic dyke, IV—North Sudetic Basin–volcanic plug from Organy, V—Intra-Sudetic Basin–tuff from Krucza Skała. A short-name is given for each locality used throughout the manuscript: I—Halle, II—Chemnitz, III—Bieberstein, IV—Organy, V—Krucze.

3. Case Study of Permo-Carboniferous Rhyolites

3.1. Geological Setting

The Variscan orogeny resulted from the collision of Gondwana and Laurasia (Devonian to Carboniferous, 380–280 Ma) with subsequent post-collisional processes involving Permian and Late Carboniferous magmatism. The magmatism comprised voluminous rhyolites and granites with minor occurrences of more mafic rocks [16,17]. The age of rhyolitic post-collisional magmatism has been known for over 20 years and U-Pb zircon ages were consistent with major episodes of eruptions taking place between 310 and 280 Ma [16].

The rhyolitic rocks chosen for this study represent diverse forms of Permo-Carboniferous volcanism in Germany and Poland (Figure 1). Generally, four of them were emplaced/erupted in sedimentary intermontane basins developing during the Permo-Carboniferous period. From those, Halle and Organy represent subvolcanic/volcanic rocks, Krucze volcanic/pyroclastic, and Chemnitz pyroclastic products. Bieberstein is a subvolcanic dyke intruding an older metamorphic basement.

The Chemnitz sample was ignimbrite containing numerous pyroclastic units that erupted within the Chemnitz Basin (which has accommodated volcano-sedimentary succession) [16]. There are abundant pyroclastic rocks related to a large caldera eruption occurrence to the north of the Chemnitz Basin in the North Saxon Volcanic Complex [18]. The Chemnitz sample was taken from so-called Planitz vitrophyre, a rock that is exceptionally well preserved and fresh with dominant glass content [9]. The sample came from a temporary outcrop in Zwickau. Previous zircon from the same outcrop has been dated using the U-Pb method and SHRIMP instrument, yielding a concordia age of 296.6 ± 3.0 Ma [16].

The Halle sample represented fully crystalline subvolcanic rhyolite from the Halle Volcanic Complex (located within the Saale Basin). The Halle Complex comprises several fine-grained and coarse-grained laccoliths [19,20] emplaced from 291.7 ± 1.8 to 301 ± 3 Ma [19]. The individual laccoliths were formed by several successive magma pulses with evidence of the prolonged laccolith formation being consistent with structural, petrological, and geochemical data [15,21,22]. The sample analyzed in this study came from coarse-grained Landsberg laccolith that was shown to contain chemically and isotopically diverse zircon of Permian age, suggesting the presence of both antecrystic and autocrystic grains [23].

The Organy sample was subvolcanic/volcanic rhyolite from the North-Sudetic Basin. The basin is filled with volcano-sedimentary succession containing a bimodal volcanic suite. The felsic rocks in the basin are dated between 288 and 298 Ma [24,25]. The Organy sample was from the Organy Wielisławskie exposure famous for its columnar jointing that represents either roots of a volcanic dome or a subvolcanic intrusion associated with rhyolitic tuffs and breccias [24]. The rhyolites were dated 297.5 ± 2.8 Ma [25] and 292–294 Ma [24]. The post-eruptive fluid migration resulted in secondary overprinting of rhyolites and strong albitization of tuffs. The hydrothermal processes and fluid migration associated with volcanic activity have been well recorded in this area, as rhyolites occurring nearby are famous for agate formation, and Au-sulphide mineralization occurs as a result of‘ the contact between Organy rhyolites and metasedimentary rocks [25].

The Krucze sample was a part of lava/tuff sequence that has been included in a thick volcano-sedimentary fill of the Intra-Sudetic Basin. The volcanic activity in the basin predominately comprises silicic rocks (rhyodacites in Carboniferous and rhyolites in Permian) and less abundant intermediate volcanic rocks [26,27]. The volcanism is dated between 313 and 283 Ma, with the peak activity at ~290 Ma. The analyzed Krucze sample also probably represented effusive/extrusive Permian volcanism, but had not been dated so far.

The Bieberstein sample came from a rhyolitic subvolcanic dyke that probably represents the feeding system of an eroded volcanic complex; however, it had not previously been studied in detail.

The choice of the samples was dictated by their diversity in texture and Zr content. In theory, we expect different structural positions of zircon in volcanic and pyroclastic rocks with variable Zr contents as well as some differences between fully crystalline and predominately non-crystalline rocks. In fact, Zr content should be the main factor controlling the appearance of zircon in crystallizing magma, as it reflects the timing of zircon saturation, while also being affected by the presence of antecrystic and xenocrystic zircons.

3.2. Chemical Composition

Rock samples from all localities were classified as rhyolite by the total alkali-silica (TAS) diagram except from one measurement from Halle that was in the trachyte field. The full dataset is presented in Supplementary Materials Table S2. SiO_2 content in rocks varied from 68 wt% in Halle to 76 wt% in Organy. Samples from all localities were enriched in LREE and had similar REE patterns (Figure 2). Only the Bieberstein rhyolite was more depleted in HREE than other rocks. Negative anomalies in Nb, Ta, Ti, Sr (Figure 2), and Eu were observed in all samples. A Sr anomaly in Chemnitz and an Eu anomaly in Bieberstein were less negative than in other samples. Zirconium content varied from 100 to

350 ppm and correlated with the average variations in zircon saturation temperatures from 780–790 °C for Halle, Bieberstein, and Organy, and 820–850 °C for Chemnitz and Krucze [28].

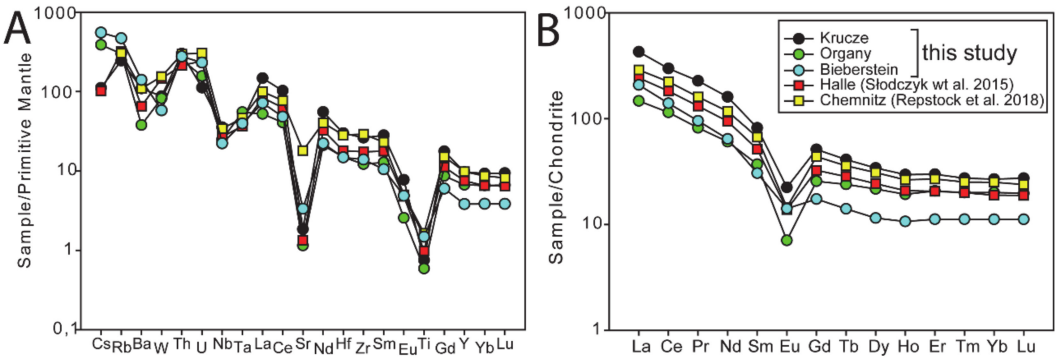

Figure 2. Whole rock composition in spider (**A**) and REE diagrams (**B**). The patterns show the averages of all analyses presented in the Supplementary Materials, with data for Chemnitz and Halle taken from Słodczyk et al. [15] and Repstock et al. [9] respectively. Reference values used to normalize the data are from Sun and McDonough [29].

3.3. Petrography

The rhyolites in all localities were dominated by fine-grained or glassy matrix (Figure 3). K-feldspar formed phenocrysts in all localities, with quartz, biotite, and plagioclase being common in most instances (Figure 3). Full modal composition is given in Supplementary Materials Table S3 and the SEM-MLA images from each section are given in Supplementary Materials Figure S1.

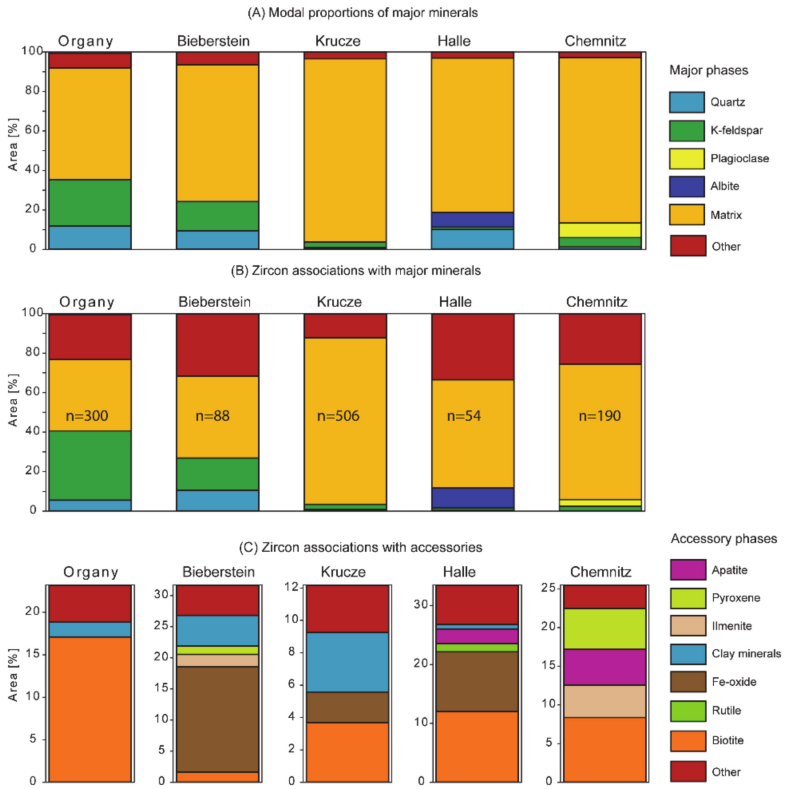

Figure 3. Modal composition and proportions of minerals associated with zircon as calculated by Mineral Liberation Analysis software. (**A**) Modal proportions of major minerals in the studied rocks; (**B**) zircon associations with major minerals in the studied rocks (*n* is the number of zircon grains detected in each sample by MLA-SEM); (**C**) zircon associations with accessory minerals in the studied rocks.

3.3.1. Chemnitz

The texture of the Chemnitz sample (Planitz ignimbrite) was vitroclastic and welded. Most of the Chemnitz ignimbrite was made up of glassy matrix (83.7%). Phenocrysts constituted approximately 16% of the ignimbrite and were dominated by plagioclase (7.4%) and K-feldspar (4.8%). Less abundant were quartz (1.2%), pyroxene (0.9%), and biotite (0.8%). These modal proportions are in excellent agreement with the MLA data from six other sections from Chemnitz ignimbrite published in Repstock et al. [9], which were also dominated by plagioclase (6.59–8.07%) and K-feldspar (4.46–6.11%), with lower abundances of quartz (1.97–2.44%), pyroxene (0.68–0.93%), and biotite (0.8–1.13%). Most phenocrysts had a size below 1 mm and usually formed sharp-edged fragments, but numerous grains, especially pyroxene and ilmenite, had rounded shapes and seemed to be resorbed (Figure 4a,b). Minerals often formed characteristic assemblages; for example, resorbed ilmenite was surrounded by biotite (Figure 5). On the other hand, pyroxene often contained or was attached to smaller ilmenite, apatite, and Fe-oxide grains, and some pyroxene was altered to actinolite. Sometimes pyroxene and plagioclase occurred as glomerocrysts (Figure 4a), and miniscule grains of various sulphides (Pb, Zn, Fe-Cu) occurred within the glomerocrysts (Figure 4a). Altogether it seems that a plutonic rock composed of pyroxene and plagioclase and abundant accessories (including zircon) was disturbed during rhyolitic magma formation and incorporated within the silicic magma.

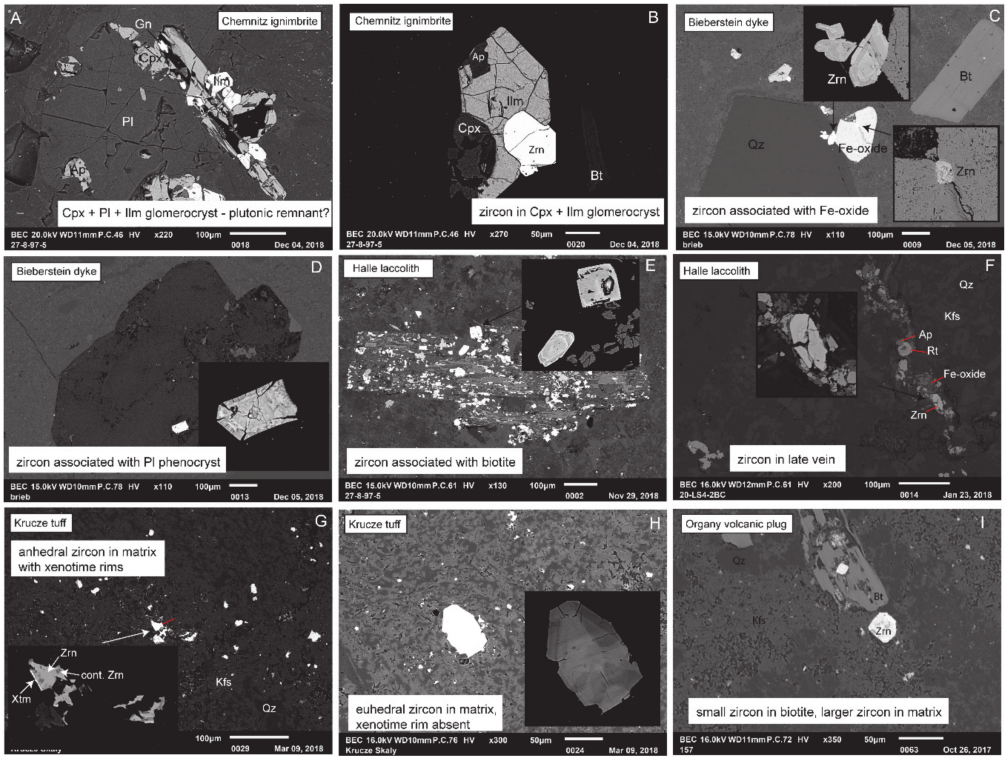

Figure 4. Back-Scattered electron (BSE) images showing typical occurrences of zircon in the studied rhyolites and corresponding images of zonation in the zircons. (**A**,**B**) BSE images of Chemnitz ignimbrite commonly showing plagioclase-pyroxene plus accessory glomerocrysts; (**C**) Bieberstein dyke, with zircon being commonly associated with Fe-oxides; (**D**) Bieberstein dyke with zircon included in altered plagioclase porphyrocryst; (**E**) Halle laccolith-zircon in biotite and matrix; (**F**) Halle laccolith-zircon associated with late veins rich in accessory phases and Fe-oxides; (**G**) Krucze sample with abundant anhedral zircon with xenotime rims; (**H**) Krucze sample with euhedral/subhedral zircon without xenotime rims; (**I**) Organy lava dome showing diverse zircon sizes within and outside biotite phenocryst. Cpx—clinopyroxene, Ilm—ilmenite, Pl—plagioclase, Ap—apatite, Zrn—zircon, Bt—biotite, Qz—quartz, Kfs—K-feldspar, Rt—rutile, Xtm—xenotime, Gn—galena.

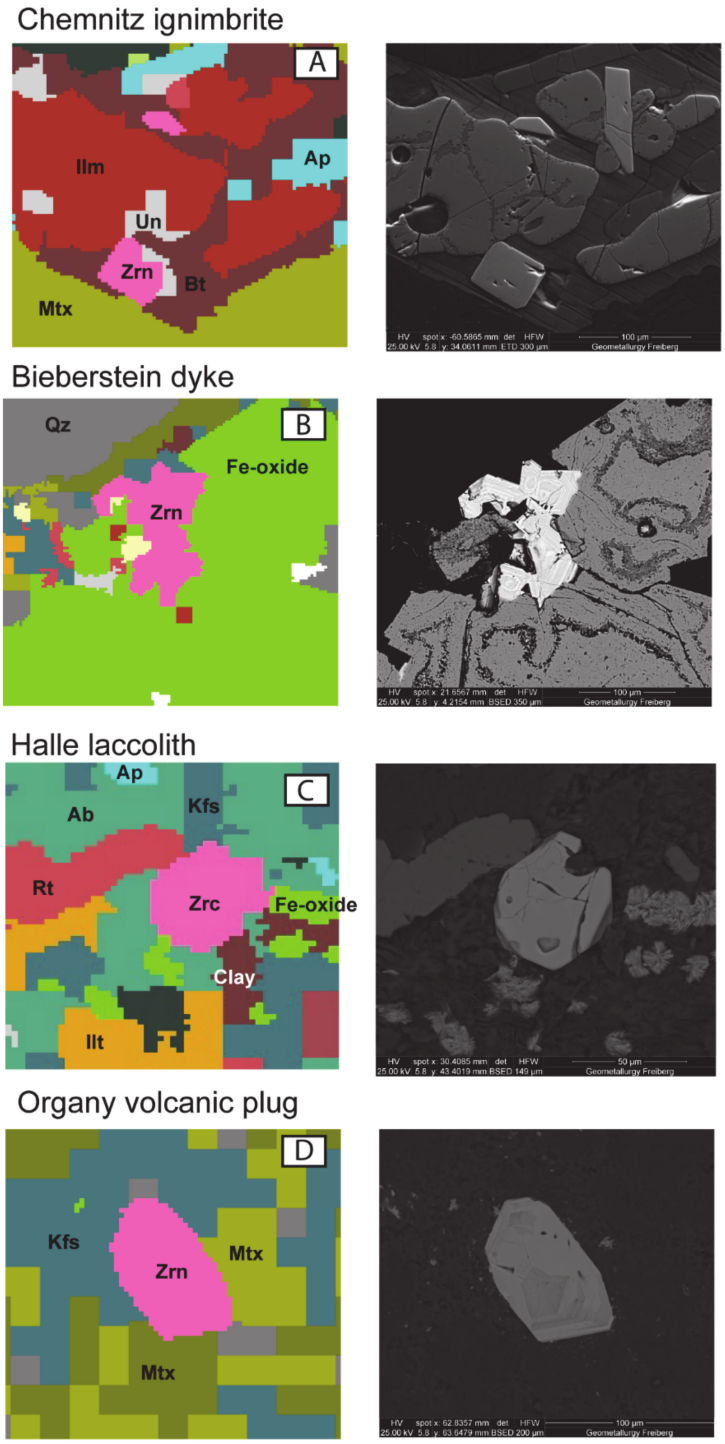

Figure 5. Examples of zircon associations in MLA images, and examples of different structural positions of zircon in BSE images. (**A**) Chemnitz ignimbrite, showing zircon and other accessories in ilmenite-rich glomerocryst. Interestingly one zircon is missing from the MLA image; however, this was the only case where this happened. (**B**) Bieberstein dyke showing the typical association of zircon with Fe-oxide. This interesting glomerocryst of several zircons was detected as a single grain by MLA. (**C**) Halle laccolith, showing zircon associated with accessory minerals in a late vein. (**D**) Organy lava dome, showing a typical matrix-associated zircon. Ilm—ilmenite, Zrn—zircon, Ap—apatite, Bt—biotite, Mtx—matrix, Un—unknown, Qz—quartz, Ab—albite, Kfs—K-feldspar, Rt—rutile, Ilt—illite, clay—clay minerals.

3.3.2. Bieberstein

The texture of the rhyolite was massive and porphyritic. Rhyolite from Bieberstein mostly contained a matrix of K-feldspar and quartz. Phenocrysts constituted 18% of the rock and were dominated by K-feldspar and quartz (Figure 4c,d). Kaolinite was less abundant (5%), and was interpreted as the alteration of plagioclase, which was confirmed by the presence of albite (0.2%) within the phenocrysts. Small biotite phenocrysts constituted 0.8% of the rhyolite. Most of the phenocrysts were subhedral and less than 1 mm, with the exception of biotite, which often was euhedral (Figure 4c). Fe-oxide, which constituted 0.12% of the area, occurred mostly as aggregates (Figure 5b), which we interpreted as fully altered pyroxene. Interestingly, zircon was often associated with Fe-oxides (Figures 4c and 5b); however, it also occurred within other phenocrysts or matrices (Figure 4d). The rock contained crosscutting quartz veins and diffuse zones enriched in K-feldspar and quartz (see the MLA image in Supplementary Materials Figure S1). Diffuse zones were ~5 mm wide and quartz veins were ~20 µm wide, which probably represented the shearing of the rhyolite in both plastic and brittle regimes. These shear zones were later infiltrated by late melts/fluids.

3.3.3. Halle

Rhyolite from Halle Volcanic Complex had a massive and porphyritic texture. It belonged to the coarse-grained rhyolite type [30]. Phenocrysts constituted 17%, with the most abundant being quartz and albite. The mineral background was a mixture of quartz, plagioclase, and K-feldspar. Accessory minerals were biotite (1.7%), Fe-oxides (0.5%), illite (0.2%), and rutile (0.13%). Quartz and biotite were anhedral, while albite was subhedral to euhedral. Biotite sometimes occurs as inclusions in quartz. Most of the phenocrysts were less than 1 mm, while larger phenocrysts (quartz and albite) reached up to 6 mm. Few quartz grains were embayed and overgrown by albite. Minerals like Fe-oxides and illite occur as an alteration after biotite, and altered biotite often contains numerous accessory phases such as zircon, apatite, and rutile (Figures 4e and 5c). For some samples (not analyzed by MLA) discontinuous vein-like structures filled with Fe-oxides and containing abundant accessory minerals were seen (Figure 4f).

3.3.4. Krucze

The texture of the Krucze sample was massive and fine-grained with very rare phenocrysts (Figure 4g,h). The rock contained ~7% phenocrysts of quartz, K-feldspar, and albite. Most of phenocrysts had a size below 100 µm, and that largest grains (quartz and albite) had sizes ~600–700 µm. Quartz and K-feldspar grains were anhedral, and there were a few subhedral albite grains. Albite is an alteration product after plagioclase, and its matrix was composed mostly of quartz and K-feldspar (Figure 4g,h). Diffuse zones enriched in quartz represented the probable infiltration of late melts/fluids. Other accessories included pyroxene, Fe-oxides, biotite, rutile, and zircon. Zircon appeared in the matrix as subhedral small grains with xenotime rims (Figure 4g) and large euhedral grains without xenotime (Figure 4h).

3.3.5. Organy

The texture of the rhyolite from Organy was massive and porphyritic. Phenocrysts constituted approximately 16% of the rhyolite. Dominating phenocrysts were K-feldspar and quartz. Less abundant were albite (2.8%) and illite (1.4%, alteration product of K-feldspar), biotite (1%), and plagioclase (0.4%). Most of the grains has a size less than 1 mm, with maximum sizes being over 3 mm (K-feldspar). The matrix was composed of quartz and K-feldspar (Figure 4i). Zircon appeared in biotite and matrix, with the latter zircon having larger sizes (Figure 4i). The rock was cracked in places, with the cracks filled mostly by kaolinite, and occasionally by Fe-oxides and illite. Two thin sections were analyzed for this locality, and MLA returned similar modal proportions and a similar grain size distribution

(Supplementary Materials Table S2, Figure 6). This, together with the low chemical variability within each locality, suggests that each sample could be treated as representative for each site.

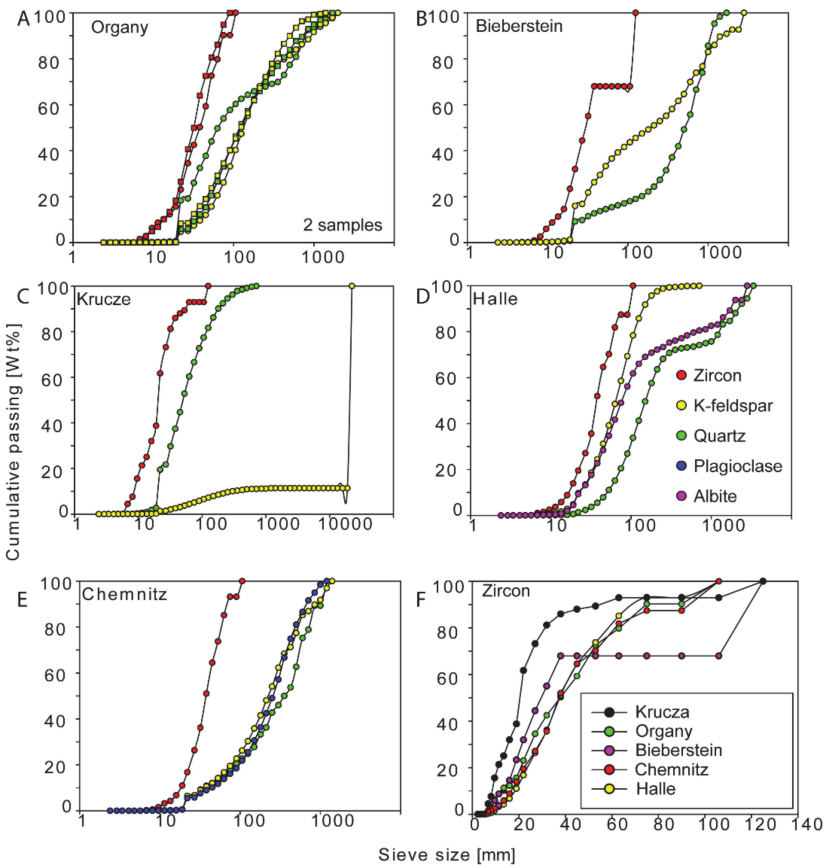

Figure 6. Grain size distribution for major minerals in each locality (**A**–**E**) as well as a comparison of zircon grain size distribution in different localities (**F**). Data are from MLA. Please note that in Krucze (**C**) fine-grained K-feldspar was recognized as a single grain by the software.

3.4. Zircon Associations

SEM-MLA can be used to detect most zircon grains and describe their structural positions and mineral associations in detail. For the analyzed sections, the number of detected grains for each section was: Organy1-25 grains, Organy2-175, Chemnitz-190, Halle-54, Beiberstein-88, Krucze-506. The majority of these grains were smaller than 50 µm in length, with the larger grains constituting 11, 8, 31, 5, 6, and 8 grains in each of the localities, respectively. Mineral association data can be correlated and checked with the BSE images of zircon grains in Figures 4 and 5.

In general, zircon associations are correlated with modal mineralogy (i.e., the more a mineral (or matrix) constitutes a larger part of the rock, then more zircon is associated with it (for details see Supplementary Materials Table S3)). In the studied rocks, zircon was commonly associated with matrix and K-feldspar. However, even zircon associated with uncommon mineral assemblages was usually partly surrounded by fine-grained matrix composed of major phases (Figure 5A–C), giving somehow false impression of zircon association with major minerals, which restricted information on its structural position. For this reason, it was important to verify each association with MLA and BSE images, which could be achieved manually after automated analyses were completed (saving the position of each zircon grain so that each zircon grain can be quickly accessed manually). For example such verification showed that in the case of zircon that was associated with K-feldspar and quartz, both major minerals were more often matrix constituents and not porphyrocrysts (Figures 4 and 5). Therefore, we suggest that in terms of identifying different structural positions of zircon in the

rock, more information is provided by zircon associations with minor and accessory minerals and not the major ones. For example, minerals such as biotite were important hosts for zircon in all samples. The association of zircon with biotite is an interesting one, because it does not follow the correlation between rock mode and mineral association (e.g., biotite constitutes only up to 1.7% of the rock mode, but over 17% of zircon is associated with biotite in Organy rhyolite). Additionally, this amount may be underestimated, because biotite is often fully altered, as in the Halle sample. Similarly apatite constitutes only up to 0.12% of the rock mode, however, in Chemnitz and Halle, much higher amounts of zircon were associated with apatite (4.6% and 2.5%, respectively). Other minerals like albite (30% in Halle), Fe-oxides (17% in Bieberstein and 10% in Halle), pyroxene (5% in Chemnitz), or kaolinite (4.7% in Bieberstein) could also be associated with zircon to a greater degree than suggested by modal proportions (Figure 3).

In fact, these diverse zircon associations were consistent with the presence of several zircon populations in a single sample. This was largely confirmed for zircons associated with ilmenite, apatite, and Fe-oxides in both Chemnitz and Bieberstein. BSE images showed that zircon associated with these minerals often occurred in glomerocrysts that probably had been derived from plutonic rocks which were later disturbed and incorporated within rhyolite. On the other hand, zircon occurring in Organy was associated with biotite—a mineral that is typical for rhyolite. Specific zircon was observed in Krucze, where most of the zircon was dismembered and anhedral within the matrix and there were also epitaxial overgrowths of xenotime. The occurrence of some Halle zircon in veins with other accessory minerals was also unusual (Figure 4).

3.5. Mineral Grain Size Distribution

MLA also provided information on the grain size distribution for each mineral. Mineral grain size distribution diagrams were similar, with most grains being smaller than 1200 μm (Figure 6a–e). However, the shapes of cumulative grain size distribution curves were different for some samples. Generally, grains below 120 μm belonged to matrices and larger grains were phenocrysts. Bieberstein, Halle, and two samples from Organy had similar grain size distributions (Figure 6a,b,d), while samples from Chemnitz and from Krucze did not. In Chemnitz ignimbrite, all grains occurred as crystal fragments surrounded glassy matrices (Figure 6e). On the other hand, Krucze contained only a few phenocrysts (Figure 6c), and the matrix consisted mostly of K-feldspar, so that individual grains could not be resolved by the SEM-MLA GXMAP mode. Zircon grain size distribution plots were similar for all samples except Krucze, because zircon grains in this rock were strongly disseminated through the matrix (Figure 4g). Additionally, the plot for Bieberstein was different for the largest grain sizes because of the zircon aggregate, which had been imaged by MLA as a single grain (Figure 5b).

Grain size distribution was also compared using statistical tests (Figure 7). In the analyzed samples, Chemnitz had a significantly larger zircon area, and Krucze had a smaller zircon area, compared to other localities (Figure 7a). No many significant differences were observed between the sizes of zircon associated with different minerals (Figure 7b–d). However, the diversity in sizes was more pronounced for Chemnitz and Halle zircons (where at least two zircon populations were identified in SEM images, see Figures 4 and 5) than for Organy (where all zircon seemed similar). Quantitative information retrieved from automated SEM analysis also included grain lengths, length to breadth ratios, and angularity. We compared all these values between sites and between different mineral associations, but not many significant differences were observed (the database used for comparison is given in Supplementary Materials Table S5).

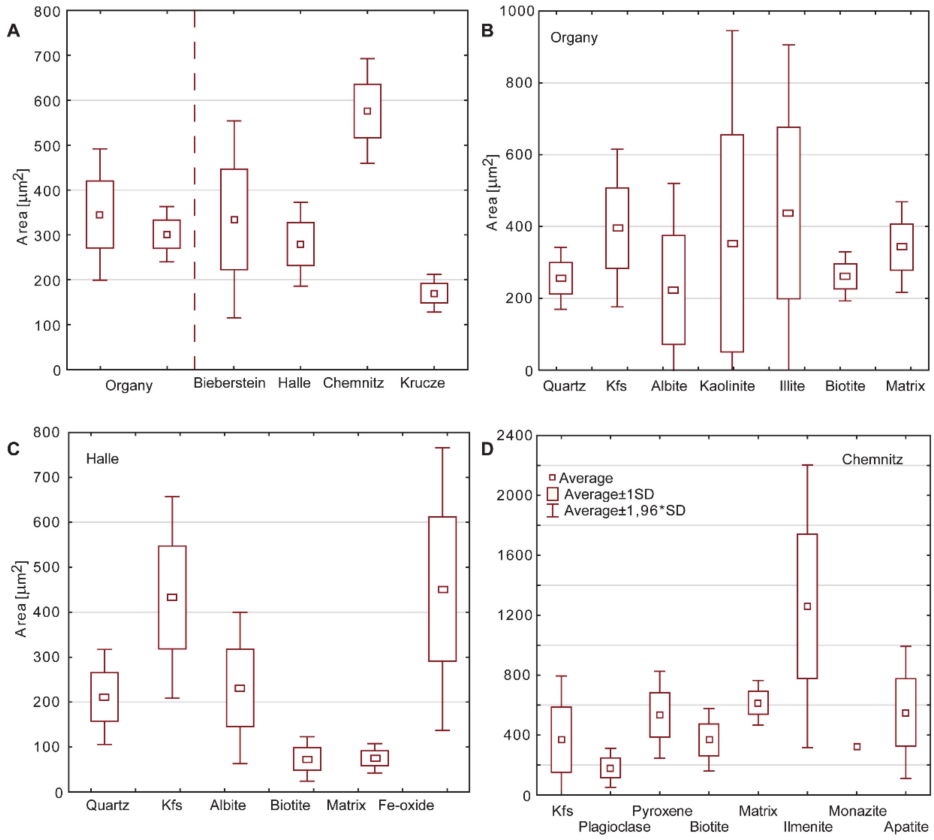

Figure 7. Statistical comparison of zircon sizes (µm^2) between localities (**A**) and between zircon associated with different minerals for each locality (**B**–**D**): (A) significant variations ($p < 0.05$) are observed for Krucze and Halle; (**B**) data do not show significant variations between populations; (**C**) zircon associated with KFs and Fe-oxide is significantly larger than zircon associated with the matrix; (**D**) data do not show significant variations between populations; however, the largest zircons are clearly associated with ilmenite. Input data from MLA, shown in Supplementary Materials. Plots made by Statistica software.

3.6. Whole-Rock Versus Modal Composition

MLA allows the concentration of an element to be compared with the quantity of a mineral that is main carrier of the element (e.g., Zr in zircon, P in apatite, and monazite and Ti in rutile and ilmenite). Generally, correlation was relatively good, especially for rocks with higher amounts of accessory minerals detected by MLA (Figure 8). As zircon was the only main carrier of Zr, it was possible to calculate the Zr content for all the zircon detected by MLA (zircon composition from Halle was used for the calculation with an average of 49 wt% of Zr [23]) and the calculated concentration was close to minimal Zr content in Halle, Krucze, and Organy whole rocks, but was much lower for Chemnitz and somewhat lower for Bieberstein.

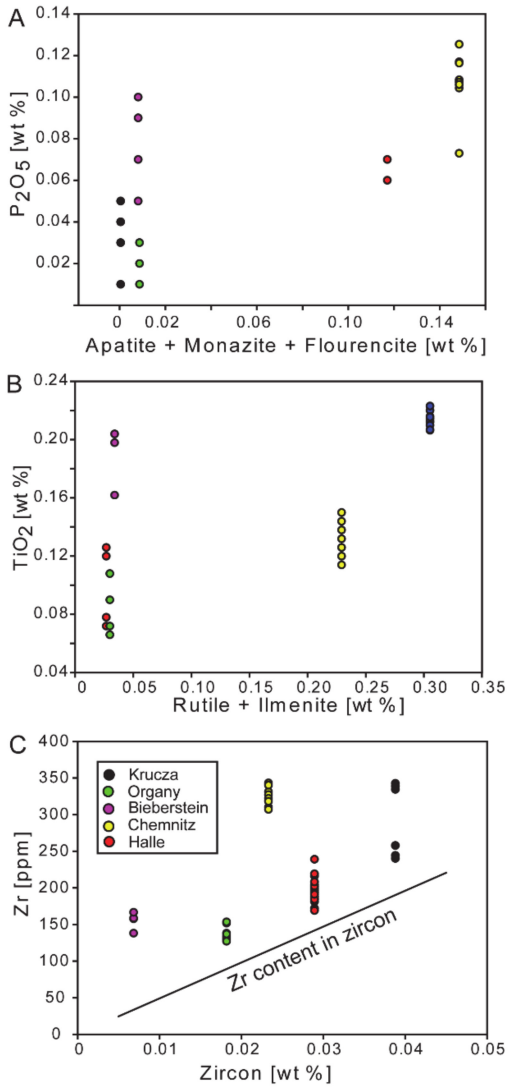

Figure 8. Comparison of modal proportions of zircon and other accessory minerals (from MLA) with whole rock compositions for the major constituents of these minerals: (**A**) phosphorous-bearing minerals, (**B**) titanium-bearing minerals (**C**) zircon**.** The solid line in the zircon diagram (C) is the expected Zr concentration in whole rock assuming that all Zr is in zircon and Zr content in zircon is the average taken from Słodczyk et al. [23].

4. Discussion

4.1. Chemical and Structural Diversity of Studied Rhyolites

The studied rhyolite rocks represented the same Permo-Carboniferous episode of intraplate volcanism related to post-Variscan extension and mantle upwelling [1,17,31,32]. In principle, they differed in the ways they were erupted/emplaced, but their chemical compositions reflected processes that should have occurred in crustal magma chambers. Differences in rhyolite chemistry and petrology are usually interpreted as reflecting a diversity of sources and differentiation processes [33–36], and that should be the case for the studied rhyolites. The studied rhyolites were compositionally homogenous within the locality and had generally similar mineral compositions as well as REE and incompatible element patterns (Figure 2). The differences in trace element contents between localities were two-to four-fold, but for immobile elements they were within the range observed in other Permo-Carboniferous rhyolites [17,18]. Therefore, the chemistry of rhyolites demonstrates some interplay between the local availability of chemically diverse source magmas and their later evolutions, which seems to be

essentially similar among the Permo-Carboniferous rhyolites in central Europe. In particular, Zr showed three-fold enrichment between localities with the range being typical not only for Permo-Carboniferous rhyolites, but also for other famous rhyolites worldwide (Figure 9). Only rhyolites or sources that were strongly affected by hydrothermal activity showed higher Zr concentrations [37,38]. However, Zr content in whole rock was not only related to magma composition, but also strongly controlled by zircon abundance (potentially including xenocrystic, inherited, antecrystic, and autocrystic components [3]), which is the case for Permo-Carboniferous rhyolites in central Europe as well [1,39]. The preservation of zircon in silicic magmas makes it a valuable tool for reconstructing silicic magma evolution. In particular, multiple sources are perfectly captured in zircon composition, which can be recycled from successive stages of magma development to end up as diverse zircon cargo in final magma chambers before eruption [1,3–5,23,40]. This diversity for Permo-Carboniferous rhyolites of central Europe was previously characterized on zircon separates [1,23,39]; however, we showed that more information on the presence and source of antecrystic/inherited components can be obtained from MLA-SEM analyses of the structural positions of zircon in thin sections of rock.

4.2. New Insights into Zircon Behavior in Silicic Magmas Based on SEM-MLA

Automated SEM analysis provides precise information on modal compositions, including the identification of many accessory phases [8,9]. However, it is the additional information such as grain size distribution and mineral association that offer better insight into the possible sources of zircon grains. Zircon from the Bieberstein dyke is a particularly good example. Its grain size distribution pattern for zircon showed large gaps in grain sizes identified in the thin section of rock that could be related to zircon glomerocryst. Such a structure is unusual for zircon crystallizing in pre-volcanic magma chambers, and should be interpreted as a fragment of a cumulate where zircon glomerocryst crystallized from intercumulus melt. Also, this zircon was associated with Fe-oxide and ilmenite that constituted only 0.13% of the rhyolite, but these minerals also formed glomerocrysts. Fe-oxides are euhedral and probably represented secondary alterations after early mafic phases (pyroxene) formed the cumulate. The fact that almost 20% of zircon was associated with these phases in the Bieberstein dyke suggests that such fragmented cumulate may be an important source of xenocrystic or antecrystic components. As such, the Bieberstein dyke contained at least two zircon populations (antecrystic components associated with Fe-oxide-rich cumulate and autocrystic components associated with matrices or phenocrysts), with quantitative information on the populations (antecrystic was at least 20%) retrieved from automated SEM analyses. Similarly, plutonic-like associations of zircon were also identified in the Chemnitz ignimbrite based on unusual associations of zircon with ilmenite, apatite, and pyroxene (15%), with all these minerals being minor phases in the rhyolite modal composition (1.2%). This suggests that these minerals were remnants of a disturbed pyroxene-plagioclase plutonic rock—perhaps an early product of the silicic magma evolution representing more-intermediate compositions. If this was the case for the Chemnitz ignimbrite, an abundance of ilmenite and apatite in the plutonic rock suggests the presence of Ti- and P-rich magmas (alkaline?), perhaps shedding more light on the initial mantle component participating in the formation of silicic volcanism.

Another source of information on zircon and in particular the timing of its crystallization relative to emplacement was the analysis of our dataset in terms of zircon proportion versus Zr content in whole rock. The positive relationship was observed for all fully crystalline samples and the proportion of zircon was consistent with Zr being predominately a zircon component. In contrast, Chemnitz ignimbrite Zr content was larger (over 300 ppm) than expected from zircon on its own (100 ppm, Figure 8). This is consistent with over 50% of Zr being in glass, which shows that zircon is a relatively late mineral in the sequence of crystallization. In contrast, apatite must have crystallized earlier, as its proportion correlated better than zircon with the total abundance of P in whole rock (Figure 8). This further implies that, in the case of Chemnitz ignimbrite, zircon saturation was not yet achieved, and most (if not all) of the zircon consisted of antecrystic components. This conclusion agrees well with the premise of zircon occurring mostly within pyroxene-plagioclase-ilmenite plutonic remnants

(Figure 4b). The zircon from the Chemnitz ignimbrite analyzed in this study (belonging to the Planitz Formation) was dated and yielded the concordia age of 296.6 ± 3.0 Ma [16]; however, samples that erupted later in the Chemnitz Basin (belonging to the Leukersdorf Formation) yielded younger ages of 291 ± 2 Ma [41]. The Planitz Formation was deposited earlier and, while the two ages are close enough, some diachronity is evident consistent with different processes involved in the magma formation. The Chemnitz ignimbrite was formed by mafic-felsic magma interactions [9], which was confirmed in our study by the presence of cumulates related to mafic rather than felsic magmatism. On the other hand, the younger samples are more felsic, contain abundant inherited zircon and Hf isotope compositions of magmatic zircon is typical for an older crust. This is consistent with the purely crustal origin of the younger rhyolites [41]. It may therefore be tentatively suggested that the Chemnitz ignimbrite analyzed in this study is older because it contains predominately the antecrystic zircon component. By analyzing zircon from this sample, we may approach ages of mafic-intermediate intrusions from ~296 Ma that, after a time period, provided heat for pervasive crustal remelting at ~291 Ma in the area.

The bimodal grain size distribution of zircon was also observed in Krucze tuff, which clearly contained at least two zircon populations—a large euhedral zircon, and small dismembered one characterized by an epitaxial growth of xenotime [42]. Unfortunately, the detection of xenotime and related quantitative information was not possible via automated SEM-MLA analyses due to the size of the overgrowths being too small. This form of anhedral zircon is puzzling, as the rock contained high amounts of Zr, but most of the zircon was in this anhedral form (506 grains detected but only eight with lengths over 50 µm), something not expected when zircon crystallizes early. Possible interpretations may include zircon dissolution or quick zircon crystallization in a foamy, erupting material. Perhaps preservation of both euhedral (antecrystic) and anhedral (autocrystic) zircon supports the latter interpretation. Dating of this rhyolite will be an analytical challenge, but one that may provide interesting results if the two populations are analyzed separately.

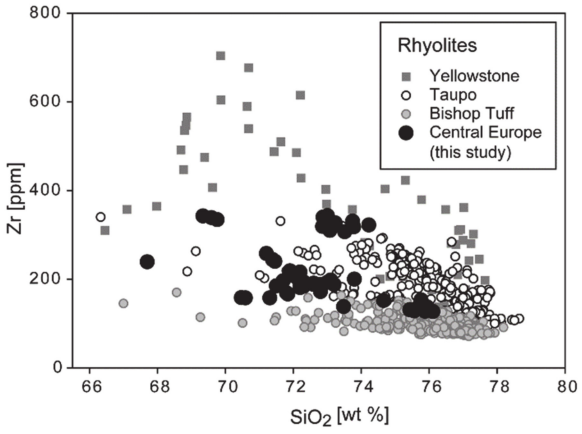

Figure 9. Comparison of whole rock SiO_2 and Zr contents in the studied rhyolites (including the whole rock composition published in [9,15] with datasets from Bishop Tuff [35], Taupo Volcanic Zone [43], and Yellowstone [38].

Zircon in Halle was often associated with other accessory minerals such as apatite, rutile, and Fe-oxide-forming veins that intruded later than the majority of the laccolith body. This would be in accordance with previous interpretations of multiple magmatic injections forming laccolith bodies [15,21,30], and would additionally suggest the presence of strongly differentiated melts during laccolith formation. As such, at least two populations occurred in Halle rhyolite—one in biotite, and one related to this later melt infiltration. In this case, both could be autocrystic or antecrystic. In fact, numerous ages obtained for laccoliths from the Halle Volcanic Complex show spreads from 292 ± 2 Ma to 301 ± 3 Ma [19], and the presence of antecrystic zircon has been suggested by Słodczyk [23] based on

zircon trace elements and isotope composition diversity. Altogether, our data also confirm prolonged and complex processes of Halle laccoliths formation.

Organy showed yet another typical zircon characteristic, the "zircon in biotite" association. Actually, this may have been the only rock containing a single zircon population that was probably related to the progressive crystallization of rhyolitic magma. This is consistent with the increasing zircon sizes from phenocrysts cores to phenocrysts rims (Figure 4i) and similar zircon sizes in different mineral associations (Figure 7). The zircon from this locality has been dated twice, with a range of ages of 297.5 ± 2.8 Ma [25] and 292–294 Ma [24], consistent with a possible presence of antecrystic zircons. However, based on our observations, we suggest that these ages may be treated as within the margin of error, or the younger ages may have been affected by lead loss related to late fluid infiltration. The spread of individual ages was 292–302 Ma [25] and 284–302 Ma [24], which is consistent with older ages being closer to the magmatic age and younger ages being affected by lead loss.

Altogether, each of the analyzed rhyolites contained zircon with different associations, showing that determining the structural position of zircon and backing it with quantitative information derived from MLA-SEM can offer a valuable tool for zircon characterization. Our survey of rhyolites with different Zr contents also confirmed that the origin of zircon in rhyolites is far from simple and rarely consistent with fully autocrystic zircon. However, at least some potential sources of antecrystic grains can be identified, usually by observing zircon associated with particular plutonic-like rock fragments.

5. Conclusions

Zircon continues to be used as the perfect mineral for dating and reconstructing magmatic and metamorphic processes. However, as it is mostly analyzed in separated grains, the information provided by its structural position within rock is lost. In this study, we showed that by observing the nature of zircon associations with other minerals, new information is obtained; for example, on zircon sources such as crystallization in volcanic rock, crystallization in earlier-formed cumulates, and crystallization in late veins. The difficulty is that zircon is scarce in thin sections of rock, and an additional tool is needed to facilitate zircon observations. We propose that the perfect approach is automated SEM analyses that provide not only qualitative information, but also quantitative data for all zircon grains in thin sections of rock. This information can be directly compared with whole rock analyses, giving it the potential for further interpretations such as the timing of zircon crystallization. We stress that such approaches may be of particular importance for rhyolitic rocks, which are known to contain diverse zircon populations. This was shown in this study, where each of five studied localities had different zircon characteristics.

Supplementary Materials: The following are available online at http://www.mdpi.com/2075-163X/10/4/308/s1, Table S1: Reproducibility of whole rock analyses based on duplicate analyses of a single sample and the reference material, accuracy of whole rock analyses based on comparison of RM analyses to the expected value; Table S2: Whole rock analyses from this study and data from References [9,15] used as a reference composition for the rocks analyzed in this study by MLA-SEM; Table S3: Modal composition as analyzed in this study by MLA-SEM; Table S4: Proportions of different minerals associated with zircon as analyzed by MLA-SEM; Table S5: Data for each zircon grain in each sample used for statistical calculations as analyzed in this study by MLA-SEM. No statistical differences were noted for Length/Breadth ratio and angularity. A single Associated mineral was chosen for one zircon grain and that was the one with maximum surface area attached to the zircon.; Figure S1: MLA images of samples analyzed in this study.

Author Contributions: Conceptualization, A.P. (Anna Pietranik); investigation A.P. (Arkadiusz Przybyło); data interpretation, A.P. (Anna Pietranik) and A.P. (Arkadiusz Przybyło); funding acquisition, A.P. (Anna Pietranik); methodology, A.P. (Arkadiusz Przybyło), B.S. and C.B.; writing—Original draft, A.P. (Anna Pietranik), A.P. (Arkadiusz Przybyło), B.S. and C.B. All authors have read and agreed to the published version of the manuscript.

Funding: The project was funded by NCN research project OPUS no. UMO-2017/25/B/ST10/00180 to Anna Pietranik.

Acknowledgments: The paper is a part of PhD dissertation of Arkadiusz Przybyło. Sabine Gilbricht is thanked for her untiring support during the automated SEM-MLA measurements at the instruments of the Geometallurgy Laboratory at the TU Bergakademie Freiberg. The very interesting Bieberstein locality could be sampled when on holiday only thanks to great landlords at the Teddy und Bummi apartaments, who lent a 5-kilo hammer. Initial ideas for importance of the structural positions of zircon within rhyolites were developed during the doctoral

thesis of Elżbieta Słodczyk and the master thesis of Angelika Tomankiewicz. Two reviewers are thanked for their comments that helped to improve the manuscript.

Conflicts of Interest: The authors declare no conflict of interest.

References

1. Pietranik, A.; Slodczyk, E.; Hawkesworth, C.J.; Breitkreuz, C.; Storey, C.D.; Whitehouse, M.; Milke, R. Heterogeneous zircon cargo involuminous late paleozoic rhyolites: Hf, oisotope and zr/hf records of plutonic tovolcanicmagma evolution. *J. Pet.* **2013**, *54*, 1483–1501. [CrossRef]
2. Schaltegger, U. Hydrothermal zircon. *Elements* **2007**, *3*, 51. [CrossRef]
3. Siégel, C.; Bryan, S.E.; Allen, C.M.; Gust, D.A. Use and abuse of zircon-based thermometers: A critical review and a recommended approach to identify antecrystic zircons. *Earth-Sci. Rev.* **2018**, *176*, 87–116. [CrossRef]
4. Bryan, S.E.; Ferrari, L.; Reiners, P.W.; Allen, C.M.; Petrone, C.M.; Ramos-rosique, A.; Campbell, I.H. New insights into crustal contributions to large-volume rhyolite generation in the mid-Tertiary Sierra Madre Occidental province, Mexico, revealed by U-Pb geochronology. *J. Pet.* **2008**, *49*, 47–77. [CrossRef]
5. Kern, J.M.; de Silva, S.L.; Schmitt, A.K.; Kaiser, J.F.; Iriarte, A.R.; Economos, R. Geochronological imaging of an episodically constructed subvolcanic batholith: U-Pb in zircon chronochemistry of the Altiplano-Puna Volcanic Complex of the Central Andes. *Geosphere* **2016**, *12*, 1054–1077. [CrossRef]
6. Słodczyk, E.; Breitkreuz, C. Zircon abundance, size and paragenesis in SiO_2-rich volcanic rocks: Implications for geochronologic studies. *Geosci. Notes* **2014**, *2.1*, 15–35.
7. Schulz, B.; Merker, G.; Gutzmer, J. Automated SEM mineral liberation analysis (MLA) with generically labelled EDX spectra in the mineral processing of rare earth element ores. *Minerals* **2019**, *9*, 527. [CrossRef]
8. Wojtulek, P.M.; Schulz, B.; Delura, K.; Dajek, M. Formation of chromitites and ferrogabbros in ultramafic and mafic members of the Variscan Ślęża ophiolite (SW Poland). *Ore Geol. Rev.* **2019**, *106*, 97–112. [CrossRef]
9. Repstock, A.; Heuer, F.; Im, J.; Hübner, M.; Schulz, B.; Breitkreuz, C.; Gilbricht, S.; Fischer, F.; Lapp, M. A Late Paleozoic Snake River-type ignimbrite (Planitz vitrophyre) in the Chemnitz Basin, Germany: Textural and compositional evidence for complex magma evolution in an intraplate setting. *J. Volcanol. Geotherm. Res.* **2019**, *369*, 35–49. [CrossRef]
10. Morrison, A.L.; Swierczek, Z.; Gulson, B.L. Visualisation and quantification of heavy metal accessibility in smelter slags: The influence of morphology on availability. *Environ. Pollut.* **2016**, *210*, 271–281. [CrossRef]
11. Pietranik, A.; Kierczak, J.; Tyszka, R.; Schulz, B. Understanding heterogeneity of a slag-derived weathered material: The role of automated SEM-EDS analyses. *Minerals* **2018**, *8*, 513. [CrossRef]
12. Klemetti, E.W.; Clynne, M.A. Localized rejuvenation of a crystal mush recorded in zircon temporal and compositional variation at the lassen volcanic center, Northern California. *PLoS ONE* **2014**, *9*, e113157. [CrossRef] [PubMed]
13. Storm, S.; Shane, P.; Schmitt, A.K.; Lindsay, J.M. Contrasting punctuated zircon growth in two syn-erupted rhyolite magmas from Tarawera volcano: Insights to crystal diversity in magmatic systems. *Earth Planet. Sci. Lett.* **2011**, *301*, 511–520. [CrossRef]
14. Keller, C.B.; Schoene, B.; Samperton, K.M. A stochastic sampling approach to zircon eruption age interpretation. *Geochem. Perspect. Lett.* **2018**, *8*, 31–35. [CrossRef]
15. Słodczyk, E.; Pietranik, A.; Breitkreuz, C.; Pedziwiatr, A.; Bokła, M.; Schab, K.; Grodzicka, M. Formation of a laccolith by magma pulses: Evidence from modal and chemical composition of the 500 m long borehole section through the Permo-Carboniferous Landsberg laccolith (Halle Volcanic Complex). *Geochem. J.* **2015**, *49*, 523–537. [CrossRef]
16. Hoffmann, U.; Breitkreuz, C.; Breiter, K.; Sergeev, S.; Stanek, K.; Tichomirowa, M. Carboniferous-Permian volcanic evolution in Central Europe-U/Pb ages of volcanic rocks in Saxony (Germany) and northern Bohemia (Czech Republic). *Int. J. Earth Sci.* **2013**, *102*, 73–99. [CrossRef]
17. Romer, R.L.; Förster, H.J.; Breitkreuz, C. Intracontinental extensional magmatism with a subduction fingerprint: The late carboniferous halle volcanic complex (Germany). *Contrib. Miner. Pet.* **2001**, *141*, 201–221. [CrossRef]
18. Repstock, A.; Breitkreuz, C.; Lapp, M.; Schulz, B. Voluminous and crystal-rich igneous rocks of the Permian Wurzen volcanic system, northern Saxony, Germany: Physical volcanology and geochemical characterization. *Int. J. Earth Sci.* **2018**, *107*, 1485–1513. [CrossRef]

19. Breitkreuz, C.; Ehling, B.C.; Sergeev, S. Chronological evolution of an intrusive/extrusive system: The late paleozoic halle volcanic complex in the northeastern saale basin (Germany). *Z. Dtsch. Ges. Geowiss.* **2009**, *160*, 173–190. [CrossRef]
20. Breitkreuz, C.; Ehling, B.C.; Pastrik, N. The Subvolcanic Units of the Late Paleozoic Halle Volcanic Complex, Germany: Geometry, Internal Textures and Emplacement Mode. In *Advances in Volcanology*; Springer: Cham, Switzerland, 2018; pp. 295–307.
21. Mock, A.; Jerram, D.A.; Breitkreuz, C. Using Quantitative Textural Analysis to Understand the Emplacement of Shallow-Level Rhyolitic Laccoliths—A Case Study from the Halle Volcanic Complex, Germany. *J. Pet.* **2003**, *44*, 833–849. [CrossRef]
22. Schmiedel, T.; Breitkreuz, C.; Görz, I.; Ehling, B.C. Geometry of laccolith margins: 2D and 3D models of the Late Paleozoic Halle Volcanic Complex (Germany). *Int. J. Earth Sci.* **2014**, *104*, 323–333. [CrossRef]
23. Słodczyk, E.; Pietranik, A.; Breitkreuz, C.; Fanning, C.M.; Anczkiewicz, R.; Ehling, B.C. Rhyolite magma evolution recorded in isotope and trace element composition of zircon from Halle Volcanic Complex. *Lithos* **2016**, *248*, 402–417. [CrossRef]
24. Awdankiewicz, M.; Kryza, R.; Szczepara, N. Timing of post-collisional volcanism in the eastern part of the Variscan Belt: Constraints from SHRIMP zircon dating of Permian rhyolites in the North-Sudetic Basin (SW Poland). *Geol. Mag.* **2014**, *151*, 611–628. [CrossRef]
25. Mikulski, S.Z.; Williams, I.S. Zircon U-Pb dating of igneous rocks in the Radzimowice and Wielisław Złotoryjski auriferous polymetallic deposits, sudetes, SW Poland. *Ann. Soc. Geol. Pol.* **2014**, *84*, 213–233.
26. Kryza, R.; Awdankiewicz, M. Ambiguous geological position of Carboniferous rhyodacites in the Intra-Sudetic basin (SW Poland) clarified by SHRIMP zircon ages. *Geol. Q.* **2012**, *56*, 55–66.
27. Awdankiewicz, M.; Awdankiewicz, H.; Rapprich, V.; Stárková, M. A permian andesitic tuff ring at Rožmitál (the Intra-Sudetic Basin, Czech Republic)—Evolution from explosive to effusive and high-level intrusive activity. *Geol. Q.* **2014**, *58*, 759–778. [CrossRef]
28. Boehnke, P.; Watson, E.B.; Trail, D.; Harrison, T.M.; Schmitt, A.K. Zircon saturation re-revisited. *Chem. Geol.* **2013**, *351*, 324–334. [CrossRef]
29. Sun, S.S.; McDonough, W.F. Chemical and isotopic systematics of oceanic basalts: Implications for mantle composition and processes. *Geol. Soc. Spec. Publ.* **1989**, *42*, 313–345. [CrossRef]
30. Breitkreuz, C.; Mock, A. Are laccolith complexes characteristic of transtensional basin systems? Examples from the Permo-Carboniferous of Central Europe. *Geol. Soc. Spec. Publ.* **2004**, *234*, 13–31. [CrossRef]
31. Breitkreuz, C.; Kennedy, A. Magmatic flare-up at the Carboniferous/Permian boundary in the NE German Basin revealed by SHRIMP zircon ages. *Tectonophysics* **1999**, *302*, 307–326. [CrossRef]
32. Benek, R.; Kramer, W.; McCann, T.; Scheck, M.; Negendank, J.F.W.; Korich, D.; Huebscher, H.D.; Bayer, U. Permo-Carboniferous magmatism of the Northeast German Basin. *Tectonophysics* **1996**, *266*, 379–404. [CrossRef]
33. Tamura, Y.; Gill, J.B.; Tollstrup, D.; Kawabata, H.; Shukuno, H.; Chang, Q.; Miyazaki, T.; Takahashi, T.; Hirahara, Y.; Kodaira, S.; et al. Silicic magmas in the Izu-Bonin oceanic arc and implications for crustal evolution. *J. Pet.* **2009**, *50*, 685–723. [CrossRef]
34. Nairn, I.A.; Shane, P.R.; Cole, J.W.; Leonard, G.J.; Self, S.; Pearson, N. Rhyolite magma processes of the ~AD 1315 Kaharoa eruption episode, Tarawera volcano, New Zealand. *J. Volcanol. Geotherm. Res.* **2004**, *131*, 265–294. [CrossRef]
35. Hildreth, W.; Wilson, C.J.N. Compositional zoning of the bishop tuff. *J. Pet.* **2007**, *48*, 951–999. [CrossRef]
36. Cole, J.W.; Deering, C.D.; Burt, R.M.; Sewell, S.; Shane, P.A.R.; Matthews, N.E. Okataina Volcanic Centre, Taupo Volcanic Zone, New Zealand: A review of volcanism and synchronous pluton development in an active, dominantly silicic caldera system. *Earth Sci. Rev.* **2014**, *128*, 1–17. [CrossRef]
37. Elliott, B.A. Petrogenesis of heavy rare earth element enriched rhyolite: Source and magmatic evolution of the round top laccolith, trans-pecos, texas. *Minerals* **2018**, *8*, 423. [CrossRef]
38. Swallow, E.J.; Wilson, C.J.N.; Myers, M.L.; Wallace, P.J.; Collins, K.S.; Smith, E.G.C. Evacuation of multiple magma bodies and the onset of caldera collapse in a supereruption, captured in glass and mineral compositions. *Contrib. Miner. Pet.* **2018**, *173*, 33. [CrossRef]
39. Słodczyk, E.; Pietranik, A.; Glynn, S.; Wiedenbeck, M.; Breitkreuz, C.; Dhuime, B. Contrasting sources of Late Paleozoic rhyolite magma in the Polish Lowlands: Evidence from U–Pb ages and Hf and O isotope composition in zircon. *Int. J. Earth Sci.* **2018**, *107*, 2065–2081. [CrossRef]

40. Chamberlain, K.J.; Wilson, C.J.N.; Wooden, J.L.; Charlier, B.L.A.; Ireland, T.R. New perspectives on the bishoptuff from zircon textures, ages andtrace elements. *J. Pet.* **2014**, *55*, 395–426. [CrossRef]
41. Luthardt, L.; Hofmann, M.; Linnemann, U.; Gerdes, A.; Marko, L.; Rößler, R. A new U–Pb zircon age and a volcanogenic model for the early Permian Chemnitz Fossil Forest. *Int. J. Earth Sci.* **2018**, *107*, 2465–2489. [CrossRef]
42. Drost, K.; Wirth, R.; Košler, J.; Fonneland Jørgensen, H.; Ntaflos, T. Chemical and structural relations of epitaxial xenotime and zircon substratum in sedimentary and hydrothermal environments: A TEM study. *Contrib. Miner. Pet.* **2013**, *165*, 737–756. [CrossRef]
43. Deering, C.D.; Cole, J.W.; Vogel, T.A. A rhyolite compositional continuum governed by lower crustal source conditions in the taupo volcanic zone, New Zealand. *J. Pet.* **2008**, *49*, 2245–2276. [CrossRef]